Research Square

Preprints are preliminary reports that have not undergone peer review.
They should not be considered conclusive, used to inform clinical practice,
or referenced by the media as validated information.

Land Surface Temperature, Vegetation and Drought Dynamics in the Forest–Savanna Transition Zone of Afadzato South District, Ghana (2006–2026): the limits of TVDI for temporal drought monitoring

Michael Akosey

makosey@gs.uesd.edu.gh

University of Environment and Sustainable Development

Fatima Eshun

University of Environment and Sustainable Development

Abraham Ackah

Kwame Nkrumah University of Science and Technology

Research Article

Keywords: Agricultural drought, Temperature–Vegetation Dryness Index, Land surface temperature, NDVI, Google Earth Engine, Drought index validation

Posted Date: November 27th, 2026

DOI: https://doi.org/10.21203/rs.3.rs-11761950/v1

License: This work is licensed under a Creative Commons Attribution 4.0 International License.
Read Full License

Additional Declarations: No competing interests reported.

Abstract

Satellite drought monitoring in data-scarce regions increasingly relies on the Temperature–Vegetation Dryness Index (TVDI), yet the index is routinely read as a time series without testing whether its construction permits temporal interpretation. Because the dry and wet edges of the NDVI–LST feature space are re-fitted to every scene, each year is internally renormalized, a property that can remove the between-year signal the index is assumed to carry. This study tests that assumption in the forest–savanna transition zone of Afadzato South District, Ghana, over the 2006–2026 dry seasons. Land surface temperature (LST) and the Normalized Difference Vegetation Index (NDVI) were derived from Landsat Collection 2 Level-2 imagery in Google Earth Engine for three decadal epochs and as a continuous annual series; TVDI was built from the NDVI–LST feature space; and each indicator was validated against Climate Hazards Group InfraRed Precipitation with Station data (CHIRPS) rainfall and ERA5-Land soil moisture. The district greened significantly (Mann–Kendall $p = 0.010$) as the surface warmed and the soil dried. Crucially, district-mean TVDI did not track the independent references across years, whereas LST correlated with rainfall and soil moisture in the physically expected direction; LST, with NDVI, is therefore the dependable temporal indicator and district-mean TVDI is not. TVDI nonetheless validated spatially, ranking land-cover types coherently from open water to built-up land and cropland. We recommend pairing an absolute thermal indicator for temporal monitoring with TVDI for spatial mapping, a transferable protocol for drought assessment in data-scarce districts of sub-Saharan Africa.

1. Introduction

Among the climate hazards that press on sub-Saharan Africa, drought ranks among the most severe. Much of the region depends on rain-fed smallholder farming, so a moisture shortfall lasting only a short time can move quickly into failed harvests, food insecurity and rural hardship (Obe et al., 2025) Ghana is no different: the drought exposure of its crop production is well established, and it differs sharply from one agro-ecological zone to another in exposure, sensitivity and capacity to adapt (Ankrah et al., 2023; Sanou et al., 2023).

The belt where the moist semi-deciduous forest of the south gives way to the drier northern savanna, the forest–savanna transition, is one of the more sensitive parts of this gradient (Njomaba et al., 2026). Its rainfall is bimodal with a marked dry season, and its farming systems work close to the limit of the moisture they can tolerate (Iseki et al., 2026), so knowing when and where dry-season moisture stress takes hold, and being able to place it spatially, is useful for early warning and for directing scarce agricultural support (Hariadi et al., 2026).

Agricultural drought is fundamentally a state of the land surface: it shows up first as a deficit of root-zone soil moisture and only later as physiological strain in the vegetation, not simply as a shortfall in rainfall (Sun et al., 2015). Optical and thermal remote sensing together record this surface expression directly (Karnieli et al., 2010). NDVI, derived from the difference between near-infrared and red

reflectance (Rouse et al., 1974), is a dependable measure of canopy greenness, but it registers water stress only with a lag, after the deficit has begun to touch the canopy. Surface temperature reacts earlier: once soil moisture runs short, evaporative cooling falls away, a larger share of energy becomes sensible heat, and the surface heats up (Fahmi et al., 2026). Combining the two offsets the delay in the vegetation signal and yields an earlier read on moisture stress (Wang et al., 2024). Plotting LST against NDVI over a large, mixed area under clear skies produces a triangular envelope, whose upper and lower edges trace the driest and wettest surfaces at each level of vegetation cover (T. Carlson, 2007; T. N. Carlson et al., 1994; Moran et al., 1994). From this, (Sandholt et al., 2002) developed TVDI, which locates each pixel between an empirically fitted dry edge and wet edge to give a dimensionless measure of surface moisture from satellite data alone. Since it needs no additional meteorological input, TVDI suits data-scarce regions, and independent datasets such as CHIRPS rainfall (Funk et al., 2015) and ERA5-Land soil moisture (Muñoz-Sabater et al., 2021) supply the references needed to test it. Comparable satellite approaches that combine NDVI, LST and rainfall variability have recently been applied to map climate vulnerability in data-scarce parts of West Africa (Álvarez & Govind, 2025).

The forest–savanna transition, and highland districts such as Afadzato South especially, are largely missing from this record. More fundamentally, although TVDI is widely applied as a drought time series, few studies test whether its per-scene renormalization permits temporal interpretation at all, or separate the temporal and spatial information the index actually carries. This study addresses both gaps. It characterizes LST, vegetation and drought in the Afadzato South forest–savanna transition zone between 2006 and 2026 and, by validating each indicator against independent rainfall and soil-moisture references, establishes which are trustworthy for temporal monitoring and which for spatial mapping. Its central contribution is to show, explicitly and against independent data, that district-mean TVDI is not a valid temporal drought indicator even though it is a sound spatial one, and to set out the complementary monitoring protocol that follows.

1. map the spatiotemporal distribution and trends of LST and NDVI over three decadal epochs (2006, 2016 and 2026) and the continuous 2006–2026 dry-season series;
2. derive TVDI and map the spatial patterns of surface moisture stress in each epoch;
3. test the reliability of TVDI and LST against CHIRPS rainfall and ERA5-Land soil moisture, and establish their complementary roles in drought monitoring; and
4. quantify temporal trends and epoch-to-epoch change with the Mann–Kendall test and Sen's slope estimator, while allowing for terrain elevation.

2. Materials and Methods

2.1 Study area

Afadzato South District sits in the Volta Region of south-eastern Ghana, on the Togo border, inside the Agumatsa sub-range of the Akwapim–Togo mountain system; Fig. 1 shows its location and terrain. The land is mostly hilly to mountainous, a mix of steep slopes, raised plateaux and lower valleys, and takes in

Mount Afadja, among the highest peaks in Ghana. That relief matters here: since temperature drops with height, the district's topography leaves a lapse-rate imprint on LST that has to be separated from variation driven by surface moisture. The climate is sub-equatorial and the rainfall bimodal, with a distinct dry season tied to the Harmattan (roughly November to March) that brings lower rainfall, shrinking minor streams and relatively clear skies. Vegetation shifts from semi-deciduous forest on the higher slopes to derived savanna grassland lower down, broken up by cultivated plots of cassava, maize, oil palm, cocoa and coffee. Because farming is largely rain-fed and smallholder, dry-season moisture stress carries real weight for local livelihoods, which is what drove the choice of study area. The patchwork of forest, savanna, cropland and settlement also supplies the spread of surface conditions needed to define the NDVI–LST feature space.

2.2 Data

The study drew on four categories of data: Landsat optical and thermal imagery for NDVI, LST and TVDI; CHIRPS rainfall (Funk et al., 2015) and ERA5-Land soil moisture(Muñoz-Sabater et al., 2021) as independent references; the Shuttle Radar Topography Mission (SRTM) Digital Elevation Model (Farr et al., 2007) for the topographic treatment; and land-cover data for class-wise interpretation. Table 1 summarizes their specifications. Every Landsat sensor was run through the shared Collection 2 Level-2 single-channel surface-temperature algorithm (Malakar et al., 2018), which delivers the cross-sensor consistency a multi-decadal comparison requires.

Table 1
Datasets and specifications.

Dataset	Product	Resolution	Period	Role
Landsat 5 TM / 7 ETM+	Collection 2 Level-2	30 m	2006 epoch / series	NDVI, LST
Landsat 8/9 OLI-TIRS	Collection 2 Level-2	30 m	2016; 2026; series	NDVI, LST
CHIRPS v2.0	Daily rainfall	≈ 5.5 km	2006–2026	Rainfall reference
ERA5-Land	Soil water, layer 1	≈ 9 km	2006–2026	Soil-moisture reference
SRTM DEM	1 Arc-Second	30 m	static	Elevation covariate
Land cover	ESA WorldCover	10 m	per epoch	Class interpretation

2.3 Image pre-processing

The processing ran in Google Earth Engine (Gorelick et al., 2017). For each epoch, and for each year of the continuous series, Collection 2 Level-2 scenes covering the district were restricted to the dry-season window (roughly December to February). Cloud, cloud shadow, cirrus and dilated-cloud pixels were screened out with the Quality Assessment (QA_PIXEL) band, following the object-based masking of (Zhu & Woodcock, 2012), and the surviving observations were combined into a median composite;

compositing over the whole dry season rather than a single date was the main defence against the persistent cloud that hampers optical–thermal work in humid tropical Ghana. Reflectance bands were rescaled to physical reflectance, and NDVI was calculated as the normalised difference of the near-infrared and red bands (Rouse et al., 1974) from the same composites as LST, so that the two variables lined up pixel-by-pixel. LST came from the Collection 2 Level-2 surface-temperature band, produced operationally from the Landsat thermal-infrared bands and validated to roughly 0.5 K (Malakar et al., 2018), then converted to degrees Celsius.

2.4 Derivation of TVDI

For each epoch, the composited NDVI and LST were combined to build the NDVI–LST feature space (Moran et al., 1994; Price, 1990). NDVI was split into narrow bins; inside each bin the highest and lowest LST marked the dry and wet edges of the envelope. The dry edge came from a linear regression of the per-bin maximum LST on NDVI ($LST_{dry} = a + b \cdot NDVI$), and the wet edge from the minimum LST (Sandholt et al., 2002). For every pixel, TVDI was calculated as $(LST - LST_{wet}) / (LST_{dry} - LST_{wet})$, running from 0 on the wet edge to 1 on the dry edge. The edges were refitted for each scene, since they depend on the atmospheric and surface conditions at the time of acquisition (T. Carlson, 2007). Figure 2 sets out the workflow.

2.5 Topographic treatment

Because the district crosses a steep elevation gradient, part of the spatial variation in LST comes from the environmental lapse rate rather than surface moisture. Elevation from the SRTM DEM(Farr et al., 2007) was kept as a covariate so that the moisture signal could be read with the elevation effect stated openly rather than blended into it.

2.6 Validation approach

The indices were tested against two independent references: dry-season rainfall from CHIRPS (Funk et al., 2015) and dry-season surface-layer soil moisture from ERA5-Land (Muñoz-Sabater et al., 2021). Since moisture stress should climb as rainfall and soil moisture drop, both TVDI and LST were expected to correlate negatively with each, in line with the validation logic for combined NDVI–LST indices set out by (Karnieli et al., 2010). The validation used the district-scale series, with results given in Section 3.4 (Table 6, Fig. 9).

2.7 Statistical and trend analysis

Relationships among the variables were measured with Pearson and Spearman rank correlation coefficients, the latter guarding against non-linearity and outliers. Change over 2006–2026 was tested with the non-parametric Mann–Kendall test (Kendall, 1975; Mann, 1945), which detects monotonic trends without assuming normality, and the size of the trend came from the Theil–Sen slope estimator (Sen, 1968). Significance was set at $\alpha = 0.05$. The three epochs were also compared by change-detection, and interannual variability was described with the coefficient of variation (CV).

2.8 Software and tools

Image retrieval, cloud masking, compositing and the calculation of NDVI, LST and TVDI were carried out with the Google Earth Engine JavaScript API (Gorelick et al., 2017). Maps were prepared in a geographic information system (QGIS), while the correlation and Mann–Kendall/Sen's slope analyses ran in Python (with the pandas, SciPy and pyMannKendall libraries), and tabular summaries were assembled in Microsoft Excel.

3. Results

The three epochs are presented as maps for their spatial patterns; the quantitative statistics come from the district-mean dry-season series (n = 21) and, for change-detection, from the three epochs.

3.1 Spatiotemporal distribution and trends of NDVI and LST

Across the 21 dry seasons, district-mean NDVI averaged 0.53 (range 0.42–0.69) and LST averaged 31.3°C (29.1–34.6°C), figures in keeping with a moderately vegetated forest–savanna surface (Table 2). Year to year, the surface variables shifted comparatively little (CV: NDVI 11.6%, LST 4.8%), whereas dry-season rainfall swung widely (mean 87 mm, CV 51%). In space, NDVI peaked over the elevated, forested northern and central districts and along the mountain chain, and fell to its lowest over the thinly vegetated, cultivated lowlands, with 2026 the greenest epoch (Fig. 3). LST ran the other way, coolest over the vegetated high ground and warmest over the valleys and settlements, and stood highest overall in 2016 (Fig. 4). Matching this pattern, LST and NDVI correlated negatively across the annual series (Pearson r = − 0.26; Table 6), the anticipated inverse link between canopy greenness and surface temperature(Fahmi et al., 2026; Karnieli et al., 2010) and the physical basis on which TVDI rests.

Table 2
Descriptive statistics of the dry-season district-mean series, 2006–2026 (n = 21).

Variable	Mean	SD	Min	Max	CV (%)
NDVI	0.526	0.061	0.421	0.688	11.6
LST (°C)	31.28	1.50	29.10	34.57	4.8
TVDI	0.469	0.054	0.347	0.570	11.5
Rainfall (mm)	87.3	44.6	30.1	209.1	51.1
Soil moisture ($m^3\ m^{-3}$)	0.237	0.028	0.195	0.285	11.9

3.2 TVDI spatial drought-stress patterns

District-mean TVDI averaged 0.47 (range 0.35–0.57). Where it earns its keep is spatially: the per-epoch maps bring out clear internal structure (Fig. 5), with moisture stress (higher TVDI, orange to red) gathering in localised lowland and less-vegetated areas and the wettest surfaces (TVDI near 0, dark blue) over valley bottoms and water bodies. Breaking TVDI down by land-cover class shows the index ordering surfaces just as physical reasoning would predict (Table 3, Fig. 6). Open water held the lowest TVDI in every epoch (0.35, 0.25 and 0.23), as expected for saturated surfaces, while built-up land and cropland held the highest, built-up reaching 0.69 in 2026 and cropland climbing across the epochs (0.51, 0.54, 0.59). Tree cover, about 58% of the district, sat at intermediate stress. This steady ordering, water wettest and built-up and cropland driest, validates TVDI against surface type and shows that the index reads relative surface moisture reliably in space.

Table 3
Mean TVDI by land-cover class and epoch (ESA WorldCover classes).

Land-cover class	2006	2016	2026	Approx. area
Tree cover	0.487	0.367	0.454	58.3%
Shrubland	0.537	0.500	0.569	28.9%
Grassland	0.539	0.518	0.558	5.6%
Cropland	0.514	0.542	0.587	2.8%
Built-up	0.564	0.493	0.686	1.6%
Water	0.353	0.248	0.234	2.7%

3.3 Temporal trends and epoch change-detection

The Mann–Kendall test paired with Sen's slope estimation (Table 4, Fig. 7) returned a single statistically significant monotonic trend: NDVI climbed across the study period ($\tau = 0.41$, $Z = 2.57$, $p = 0.010$) at + 0.0056 yr^{-1}, gaining roughly 0.11 NDVI units over two decades. LST edged upward without reaching significance ($\tau = 0.23$, $p = 0.156$; +0.11°C yr^{-1}), and TVDI did much the same ($p = 0.139$). No trend appeared in rainfall ($p = 0.65$), whereas soil moisture slipped just short of significance ($\tau = -0.29$, $p = 0.075$). Read together, the series depicts a district that turned distinctly greener and, more tentatively, warmer and drier in its topsoil.

Table 4
Mann–Kendall and Sen's slope trend results (2006–2026, n = 21).

Variable	Kendall τ	Z	p-value	Sen slope / yr	Trend
NDVI	0.41	2.57	0.010	+ 0.0056	significant increase
LST (°C)	0.23	1.42	0.156	+ 0.109	increase (n.s.)
TVDI	0.24	1.48	0.139	+ 0.0030	increase (n.s.)
Rainfall (mm)	−0.08	−0.45	0.651	−1.010	no trend
Soil moisture	−0.29	−1.78	0.075	−0.0021	decrease (marginal)

The three decadal snapshots (Table 5, Fig. 8) catch the district under contrasting conditions. From 2006 to 2026, NDVI climbed by 40%, LST dropped by 1.5°C and rainfall more than doubled, while TVDI barely moved. These snapshots are best read alongside the continuous series: 2016 landed in a dry year and 2026 in a wet one, so the epochs sample the span of conditions the district sees, while the 21-year Mann–Kendall analysis pins down the underlying trend. Taken this way, the epochs and the continuous series work together, the epochs showing where drought stress sits in space under wet and dry states, and the series quantifying change over time.

Table 5
Three-epoch comparison.

Variable	2006	2016	2026	Δ 2006→2026
NDVI	0.493	0.461	0.688	+ 0.195
LST (°C)	30.62	32.35	29.10	−1.53
TVDI	0.503	0.418	0.494	−0.009
Rainfall (mm)	94.6	30.1	209.1	+ 114.4
Soil moisture	0.272	0.202	0.256	−0.015

3.4 Reliability of the indices against CHIRPS and ERA5-Land

Set against the independent references (Table 6, Fig. 9), LST behaved as physical reasoning predicts, correlating negatively with rainfall (r = − 0.40, p = 0.07) and with soil moisture (r = − 0.35), which confirms its value as a temporal drought indicator: drier, less-watered years ran warmer at the surface. The LST–NDVI coupling carried the same expected negative sign (r = − 0.26). District-mean TVDI, by contrast, did not follow the references from year to year, because its per-scene normalisation rescales each year internally and strips out the between-year signal, which is why, as Section 3.2 shows, TVDI is informative in space rather than as a district-mean time series. The two indices are therefore complementary: LST and NDVI hold the temporal signal, and TVDI holds the spatial one.

Table 6
Correlations of the indices with the independent references (n = 21).

Relationship	Pearson r	p-value	Spearman ρ	Expected	Outcome
LST vs rainfall	−0.40	0.07	−0.35	negative	holds
LST vs soil moisture	−0.35	0.12	,	negative	holds
LST vs NDVI (coupling)	−0.26	0.26	−0.25	negative	holds
TVDI vs rainfall	+ 0.28	0.23	+ 0.37	negative	spatial index (see 3.2)
TVDI vs soil moisture	0.00	1.00	+ 0.07	negative	spatial index (see 3.2)

4. Discussion

4.1 Vegetation greening and surface warming

The strongest signal in the record is a statistically significant rise in dry-season NDVI, a greening of the district's forest–savanna surface over two decades (Ashiagbor et al., 2025; Njomaba et al., 2026). Since rainfall showed no matching trend, the greening is unlikely to be a straightforward response to higher precipitation and more probably reflects vegetation recovery, changes in land management and the accumulated effect of antecedent moisture (Wang et al., 2024). The result fits comfortably with the broader evidence of vegetation change across West Africa's transition zones, where woody cover and canopy greenness track management and multi-year moisture history as much as any single season's rainfall(Njomaba et al., 2026). The greening came with a modest surface warming, and the two connect through the vegetation–temperature coupling: across the annual series, LST and NDVI correlated negatively (r = − 0.26), and the maps show the same inverse layout in space, cooler where greener (Fig. 3, Fig. 4), in line with recent Sahelian evidence of a strong inverse vegetation–temperature coupling from NDVI and LST (Álvarez & Govind, 2025). This is the behaviour expected of the NDVI–LST relationship (Fahmi et al., 2026; Karnieli et al., 2010) and it is the physical basis on which TVDI is built (Sandholt et al., 2002). The greening trend is a solid one: significant at the 21-year scale, coherent in space, and in line with regional findings, and the harmonized Collection 2 Level-2 product used across sensors (Malakar et al., 2018) keeps the comparison valid over the full period. The district also makes an instructive contrast with Ghana's urban surfaces, where warming is driven by the loss of vegetation to built-up growth (Athukorala & Murayama, 2020; Gyile et al., 2025); here the rural transition zone greened while warming only modestly, a sign that transition-zone dynamics behave differently from the urban case and deserve study on their own terms.

4.2 TVDI and spatial drought-stress patterns

TVDI resolved the spatial pattern of moisture stress across the district clearly and consistently, which is exactly what the index was built to do (T. Carlson, 2007; Sandholt et al., 2002). The land-cover breakdown gives direct evidence that this spatial signal can be trusted: in every epoch TVDI placed surfaces in the

physically correct order, open water the wettest and built-up land and cropland the driest (Table 3, Fig. 6). That ordering validates the index against surface type and echoes the way TVDI has been used elsewhere to tell wet and dry surfaces apart within a scene (Karnieli et al., 2010; Moran et al., 1994; Price, 1990). The steadiness of the district-mean value follows from how the index is built: the dry and wet edges are refitted to each scene, so every year is normalized internally (T. Carlson, 2007), which is precisely why TVDI is read spatially, as a within-scene map of relative stress, rather than as a district average. The consistently higher TVDI over cropland is striking in a rain-fed farming district (Antwi-Agyei et al., 2012; Iseki et al., 2026): it flags cultivated land as the surface under the greatest dry-season moisture stress, which is directly useful for targeting agricultural support. Because a single land-cover map was applied to every epoch, the cropland pattern is best confirmed in later work using epoch-specific land cover.

4.3 Complementary indicators for drought monitoring

The validation shows the two indicators playing complementary roles, and that is the study's central practical result. LST correlated negatively with both rainfall and soil moisture, just as the surface energy balance implies, since less moisture curbs evaporative cooling and pushes surface temperature up (Karnieli et al., 2010; Sun et al., 2015; Zhou et al., 2022); this makes LST, alongside NDVI, a reliable indicator of drought dynamics over time. TVDI, being a relative within-scene index by construction, adds the spatial dimension, mapping where stress concentrates within each epoch. The indicators do not compete so much as combine: LST and NDVI say when the district is under stress, and TVDI says where. Read together they give a fuller drought picture than any single index, and it is this pairing, rarely applied in Ghana's transition zones, that the present study puts to work. The result also carries a portable design lesson for data-scarce regions: match an absolute, physically anchored variable such as LST for temporal monitoring with a relative index such as TVDI for spatial mapping (Zhou et al., 2022).

4.4 Temporal trends and decadal change

The trend analysis backs a consistent picture of a greening district that is slowly warming and drying. NDVI reached significance, and while the LST warming and the soil-moisture decline did not, both lean the same way and fit a slow drying tendency running beneath high interannual rainfall variability (CV 51%) (Ankrah et al., 2023). That variability is itself a notable regional finding, in line with reports of increasingly variable and extreme rainfall across southern Ghana. The decadal snapshots round out the trend: 2016 caught the district in a dry year and 2026 in a wet one, so together the epochs document the spatial pattern of drought stress across the range of conditions the district meets, while the continuous Mann–Kendall and Sen's slope analysis (Kendall, 1975; Mann, 1945; Sen, 1968) fixes the direction and rate of change over time. The two views reinforce one another: the maps pin down stress under contrasting states, and the series confirms the underlying greening. Pairing decadal mapping with continuous trend analysis is what lets the study speak to both the where and the when of drought in the district.

4.5 Limitations of the study

Several limitations qualify these findings. First, a single land-cover map (ESA WorldCover) was applied to all three epochs, so the land-cover TVDI ordering, and in particular the high cropland stress, should be confirmed in future work using epoch-specific land cover. Second, the independent references are much coarser than the 30 m Landsat indices, CHIRPS at about 5.5 km and ERA5-Land at about 9 km, so the validation carries a scale mismatch that smooths out fine spatial detail. Third, validation was performed on district-mean annual values (n = 21); the surface warming and soil-moisture decline, though consistent in direction, did not reach significance at this scale.

Fourth, although dry-season median compositing reduced cloud contamination, residual cloud effects cannot be fully excluded in the humid tropics, and the optical–thermal record remains sparser here than in drier regions. Fifth, the three decadal epochs sample contrasting weather states, 2016 fell in a dry year and 2026 in a wet one, so epoch-to-epoch differences reflect interannual variability rather than independent points on a trend; the continuous 21-year series, not the epochs, carries the trend signal. Finally, the central finding that district-mean TVDI is not a valid temporal indicator is itself scale-specific: it concerns the district-mean time series produced by per-scene renormalization and does not question the established value of TVDI as a within-scene spatial index.

5. Conclusion

This study set out to test, rather than assume, how the Temperature–Vegetation Dryness Index should be used for drought monitoring, with the forest–savanna transition zone of Afadzato South District as the case. Its central result is a cautionary one: district-mean TVDI did not track independent rainfall and soil-moisture references through time, because its per-scene renormalization removes the between-year signal, so it should not be read as a temporal drought index even though it remains a reliable spatial one. Significant greening ran through 2006–2026, NDVI peaking over the forested highlands while LST held the opposite spatial pattern, at its warmest over the thinly vegetated lowlands. In every epoch TVDI charted where dry-season moisture stress fell and sorted land-cover types sensibly, water at the wet end and built-up land and cropland at the dry end, which bears out its worth for spatial drought mapping. LST moved with rainfall and soil moisture as physics would predict and, together with NDVI, proved the steadier gauge of drought over time, whereas TVDI carried the spatial detail; the two are complementary rather than interchangeable. The Mann–Kendall and Sen's slope analysis established a significant greening trend alongside weaker warming and drying tendencies, all set against high interannual rainfall variability. Together, the results show that pairing an absolute thermal indicator for temporal monitoring with a relative index for spatial mapping gives a fuller account of drought than either on its own, and offers a practical template for drought assessment in data-scarce highland districts of sub-Saharan Africa.

6. Recommendations

The recommendations below follow from the findings and are directed at the institutions best placed to act on them:

1. The Ghana Meteorological Agency and the Water Research Institute should fold satellite LST and NDVI, which this study found to track independent moisture references reliably, into national dry-season drought monitoring, complementing the sparse rain-gauge network.
2. The Afadzato South District Directorate of the Ministry of Food and Agriculture should draw on the per-epoch TVDI drought-stress maps to steer extension services and irrigation planning towards the cropland lowlands this study marks out as the surfaces under the heaviest moisture stress.
3. The Environmental Protection Authority and district planning authorities should take the significant greening, along with the warming and drying signals, as a reference baseline for watching land-cover and climate change in the district, revising it as more imagery becomes available.

Declarations

Funding. This research did not receive any specific grant from funding agencies in the public, commercial, or not-for-profit sectors.

Competing interests. The authors declare that they have no competing interests.

Ethics approval. Not applicable. This study did not involve human participants or animals; it used only openly available satellite and reanalysis datasets.

Consent to participate. Not applicable.

Consent for publication. Not applicable.

Data availability. This study used openly available datasets: Landsat Collection 2 Level-2 imagery (accessed through Google Earth Engine), CHIRPS rainfall, ERA5-Land soil moisture, the SRTM digital elevation model and ESA WorldCover land cover. The derived dry-season series and the analysis scripts that support the findings are available from the corresponding author on reasonable request.

Author contributions. Michael Akosey: conceptualization, methodology, software, formal analysis, data curation, visualization, writing – original draft. Fatima Eshun: conceptualization, supervision, validation, writing – review and editing. Abraham Ackah: investigation, resources, data curation, writing – review and editing. All authors read and approved the final manuscript.

Use of generative AI. During the preparation of this work the authors used a generative AI language tool to improve the readability and language of the manuscript. After using this tool, the authors reviewed and edited the content as needed and take full responsibility for the content of the publication.

References

1. Álvarez, C. I., & Govind, A. (2025). Environmental and climate variability in Senegal over the last two decades: A remote sensing approach to assessing climate vulnerability in a Sahelian country.

Remote Sensing Applications: Society and Environment, *38*, 101584. https://doi.org/10.1016/j.rsase.2025.101584

2. Ankrah, J., Monteiro, A., & Madureira, H. (2023). Extreme temperature and rainfall events and future climate change projections in the coastal savannah agroecological zone of Ghana. *Atmosphere*, *14*(2), 386. https://doi.org/10.3390/atmos14020386
3. Antwi-Agyei, P., Fraser, E. D. G., Dougill, A. J., Stringer, L. C., & Simelton, E. (2012). Mapping the vulnerability of crop production to drought in Ghana using rainfall, yield and socioeconomic data. *Applied Geography*, *32*(2), 324–334. https://doi.org/10.1016/j.apgeog.2011.06.010
4. Ashiagbor, G., Ahorlu, O. E., Essah, I. S., Gyamfi, M. O., & Asabere, S. B. (2025). A remote sensing approach for mapping teak (Tectona grandis) using vegetation phenology in Ghana's forest-savannah transition zone. *Heliyon*, *11*(17).
5. Athukorala, D., & Murayama, Y. (2020). Spatial variation of land use/cover composition and impact on surface urban heat island in a tropical sub-Saharan city of Accra, Ghana. *Sustainability*, *12*(19), 7953. https://doi.org/10.3390/su12197953
6. Carlson, T. (2007). An overview of the "triangle method" for estimating surface evapotranspiration and soil moisture from satellite imagery. *Sensors*, *7*(8), 1612–1629. https://doi.org/10.3390/s7081612
7. Carlson, T. N., Gillies, R. R., & Perry, E. M. (1994). A method to make use of thermal infrared temperature and NDVI measurements to infer surface soil water content and fractional vegetation cover. *Remote Sensing Reviews*, *9*(1–2), 161–173. https://doi.org/10.1080/02757259409532220
8. Fahmi, M., Achmad, A., Husin, H., & Dewi, C. (2026). Investigating land surface temperature (LST) and its influencing factors in the Laut Tawar sub-watershed, Indonesia, using Landsat 9 data. *Sustainability*, *18*(1), 96. https://doi.org/10.3390/su18010096
9. Farr, T. G., Rosen, P. A., Caro, E., Crippen, R., Duren, R., Hensley, S., & Alsdorf, D. (2007). The Shuttle Radar Topography Mission. *Reviews of Geophysics*, *45*(2), RG2004. https://doi.org/10.1029/2005RG000183
10. Funk, C., Peterson, P., Landsfeld, M., Pedreros, D., Verdin, J., Shukla, S., & Michaelsen, J. (2015). The climate hazards infrared precipitation with stations, a new environmental record for monitoring extremes. *Scientific Data*, *2*, 150066. https://doi.org/10.1038/sdata.2015.66
11. Gorelick, N., Hancher, M., Dixon, M., Ilyushchenko, S., Thau, D., & Moore, R. (2017). Google Earth Engine: Planetary-scale geospatial analysis for everyone. *Remote Sensing of Environment*, *202*, 18–27. https://doi.org/10.1016/j.rse.2017.06.031
12. Gyile, D. N., Asare, A., Osei-Gyabaah, A. P., & Anaafo, D. (2025). Assessment of land use and land cover changes and their impact on land surface temperature in Greater Accra, Ghana. *Scientific African*. https://www.sciencedirect.com/science/article/pii/S2468227625002959
13. Hariadi, M., Sutanto, S. J., van der Schrier, G., Supit, I., Ratri, D., Steeneveld, G.-J., & Klein Tank, A. (2026). Unravelling the impact of changing rainy seasons on rice production in Southeast Asia: A

climate change high-resolution perspective. *Climatic Change*, *179*, 1. https://doi.org/10.1007/s10584-026-04136-1

14. Iseki, K., Ikazaki, K., Iizumi, T., Kobayashi, S., & Batieno, B. J. (2026). Soil heterogeneity as a key determinant of climate change impacts and adaptation for food security in the Sudan Savanna of West Africa. *Plant Production Science*. Advance online publication.
15. Karnieli, A., Agam, N., Pinker, R. T., Anderson, M., Imhoff, M. L., Gutman, G. G., & Goldberg, A. (2010). Use of NDVI and land surface temperature for drought assessment: Merits and limitations. *Journal of Climate*, *23*(3), 618–633. https://doi.org/10.1175/2009JCLI2900.1
16. Kendall, M. G. (1975). *Rank correlation methods*(4th ed.). Charles Griffin.
17. Malakar, N. K., Hulley, G. C., Hook, S. J., Laraby, K., Cook, M., & Schott, J. R. (2018). An operational land surface temperature product for Landsat thermal data: Methodology and validation. *IEEE Transactions on Geoscience and Remote Sensing*, *56*(10), 5717–5735. https://doi.org/10.1109/TGRS.2018.2824828
18. Mann, H. B. (1945). Nonparametric tests against trend. *Econometrica*, *13*(3), 245–259. https://doi.org/10.2307/1907187
19. Moran, M. S., Clarke, T. R., Inoue, Y., & Vidal, A. (1994). Estimating crop water deficit using the relation between surface-air temperature and spectral vegetation index. *Remote Sensing of Environment*, *49*(3), 246–263. https://doi.org/10.1016/0034-4257(94)90020-5
20. Muñoz-Sabater, J., Dutra, E., Agustí-Panareda, A., Albergel, C., Arduini, G., Balsamo, G., & Thépaut, J.-N. (2021). ERA5-Land: A state-of-the-art global reanalysis dataset for land applications. *Earth System Science Data*, *13*(9), 4349–4383. https://doi.org/10.5194/essd-13-4349-2021
21. Njomaba, E., Aikins, B. E., & Surový, P. (2026). Effect of climatic aridity on above-ground biomass, modulated by forest fragmentation and biodiversity in Ghana. *Earth*, *7*(1), Article 7. https://doi.org/10.3390/earth7010007
22. Obe, M. M., Kpadé, C. P., & Singbo, A. (2025). Identifying and overcoming barriers to climate change adaptation innovations among smallholder farmers in developing countries: A literature review and meta-analysis. *Climatic Change*, *178*(3), Article 49. https://doi.org/10.1007/s10584-025-03892-w
23. Price, J. C. (1990). Using spatial context in satellite data to infer regional scale evapotranspiration. *IEEE Transactions on Geoscience and Remote Sensing*, *28*(5), 940–948. https://doi.org/10.1109/36.58983
24. Rouse, J. W., Haas, R. H., Schell, J. A., & Deering, D. W. (1974). Monitoring vegetation systems in the Great Plains with ERTS. *Third ERTS Symposium, NASA SP-351*, *1*, 309–317.
25. Sandholt, I., Rasmussen, K., & Andersen, J. (2002). A simple interpretation of the surface temperature/vegetation index space for assessment of surface moisture status. *Remote Sensing of Environment*, *79*(2–3), 213–224. https://doi.org/10.1016/S0034-4257(01)00274-7
26. Sanou, C. L., Agodzo, S. K., Bessah, E., & Antwi-Agyei, P. (2023). Assessing crop–livestock water productivity in mixed-farming systems across climatic zones of Burkina Faso. *Water Practice and Technology*, *18*(11), 2577–2591. https://doi.org/10.2166/wpt.2023.162

27. Sen, P. K. (1968). Estimates of the regression coefficient based on Kendall's tau. *Journal of the American Statistical Association*, *63*(324), 1379–1389. https://doi.org/10.1080/01621459.1968.10480934
28. Sun, Y., Fu, R., Dickinson, R., Joiner, J., Frankenberg, C., Gu, L., & Fernando, N. (2015). Drought onset mechanisms revealed by satellite solar-induced chlorophyll fluorescence: Insights from two contrasting extreme events. *Journal of Geophysical Research: Biogeosciences*, *120*(11), 2427–2440. https://doi.org/10.1002/2015JG003150
29. Wang, J., Bao, Z., Wang, G., Liu, C., Xie, M., Wang, B., & Zhang, J. (2024). The time lag effects and interaction among climate, soil moisture, and vegetation from in-situ monitoring measurements across China. *Remote Sensing*, *16*(12), 2063. https://doi.org/10.3390/rs16122063
30. Zhou, W., Yu, W., Qian, Y., Han, L., Pickett, S. T. A., Wang, J., Li, W., & Ouyang, Z. (2022). Beyond city expansion: Multi-scale environmental impacts of urban megaregion formation in China. *National Science Review*, *9*(1). https://doi.org/10.1093/nsr/nwab107
31. Zhu, Z., & Woodcock, C. E. (2012). Object-based cloud and cloud shadow detection in Landsat imagery. *Remote Sensing of Environment*, *118*, 83–94. https://doi.org/10.1016/j.rse.2011.10.028

Figures

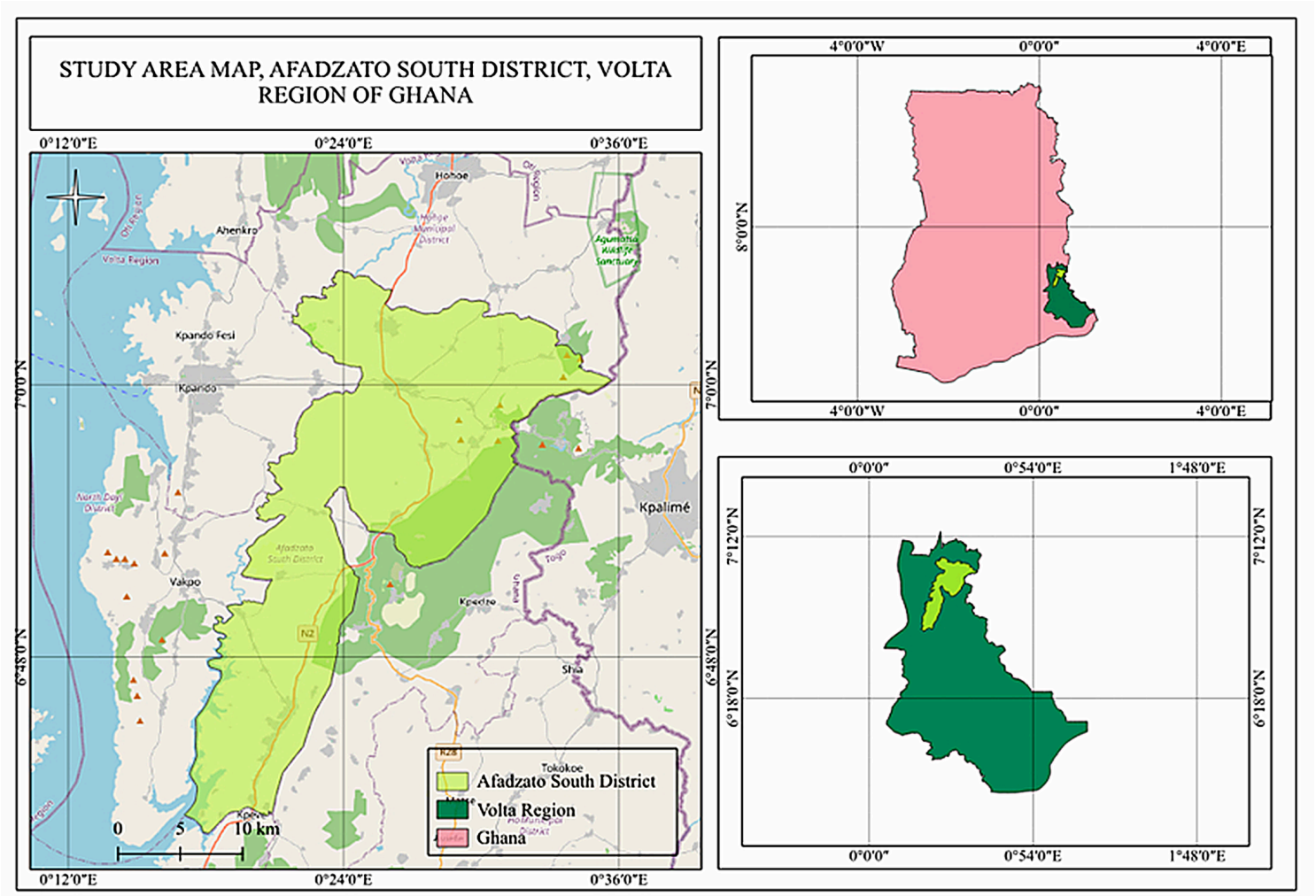


Figure 1

Location and terrain of Afadzato South District, Volta Region, Ghana.

Note: map lines delineate study areas and do not necessarily depict accepted national boundaries.

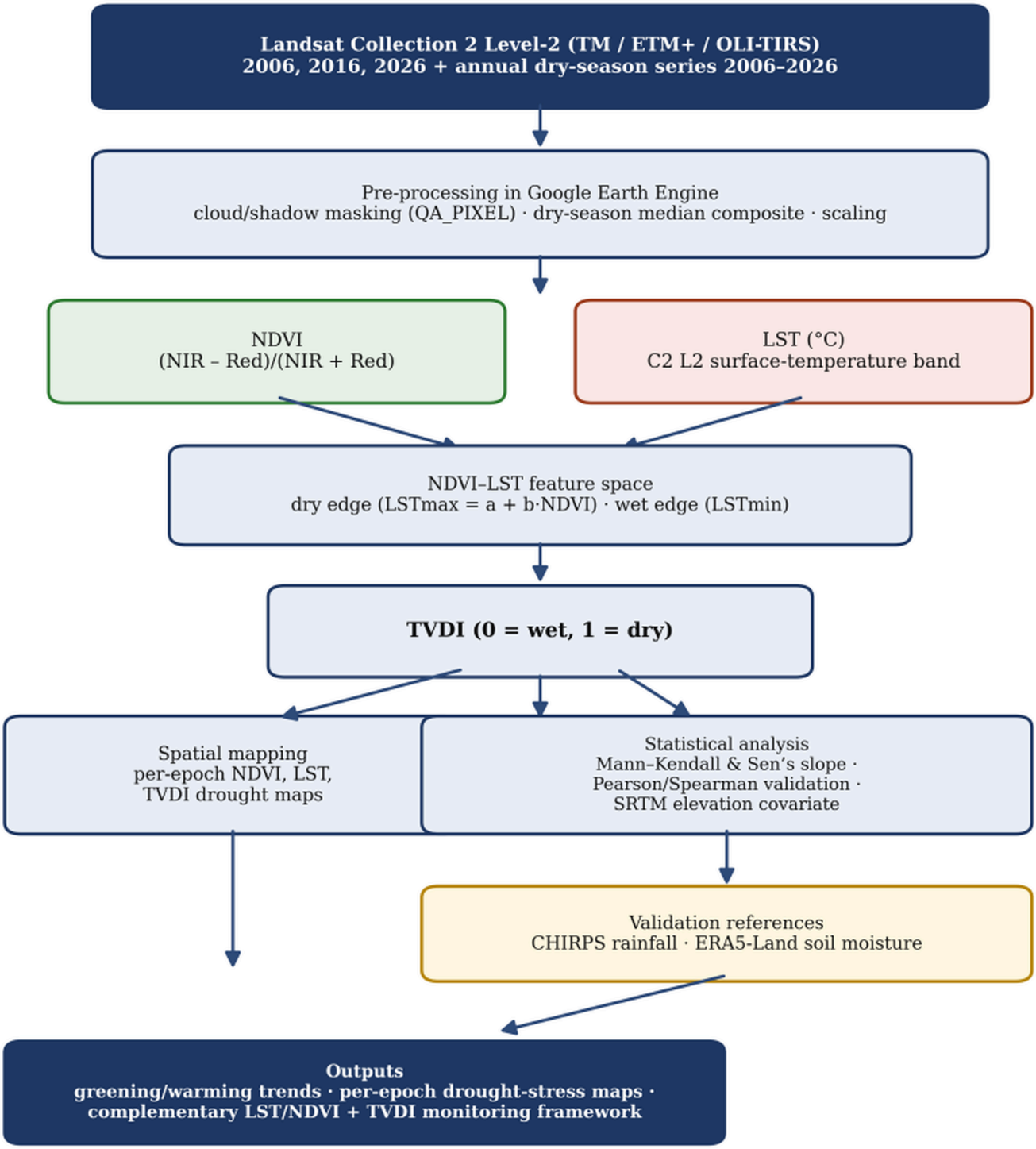


Figure 2

Analytical workflow, from Landsat inputs through NDVI, LST and TVDI to trend analysis, spatial mapping and validation.

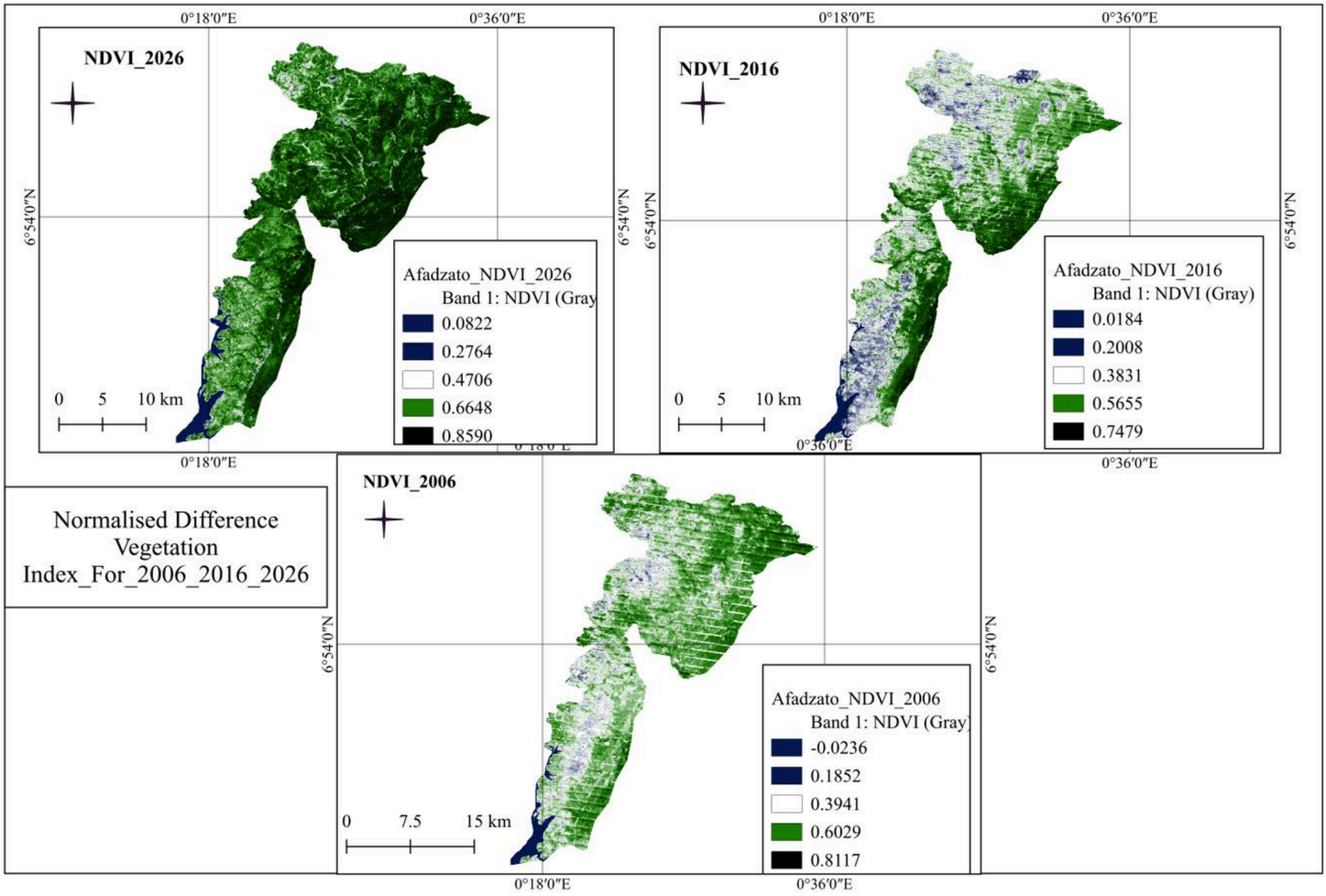


Figure 3

Dry-season NDVI for 2006, 2016 and 2026.

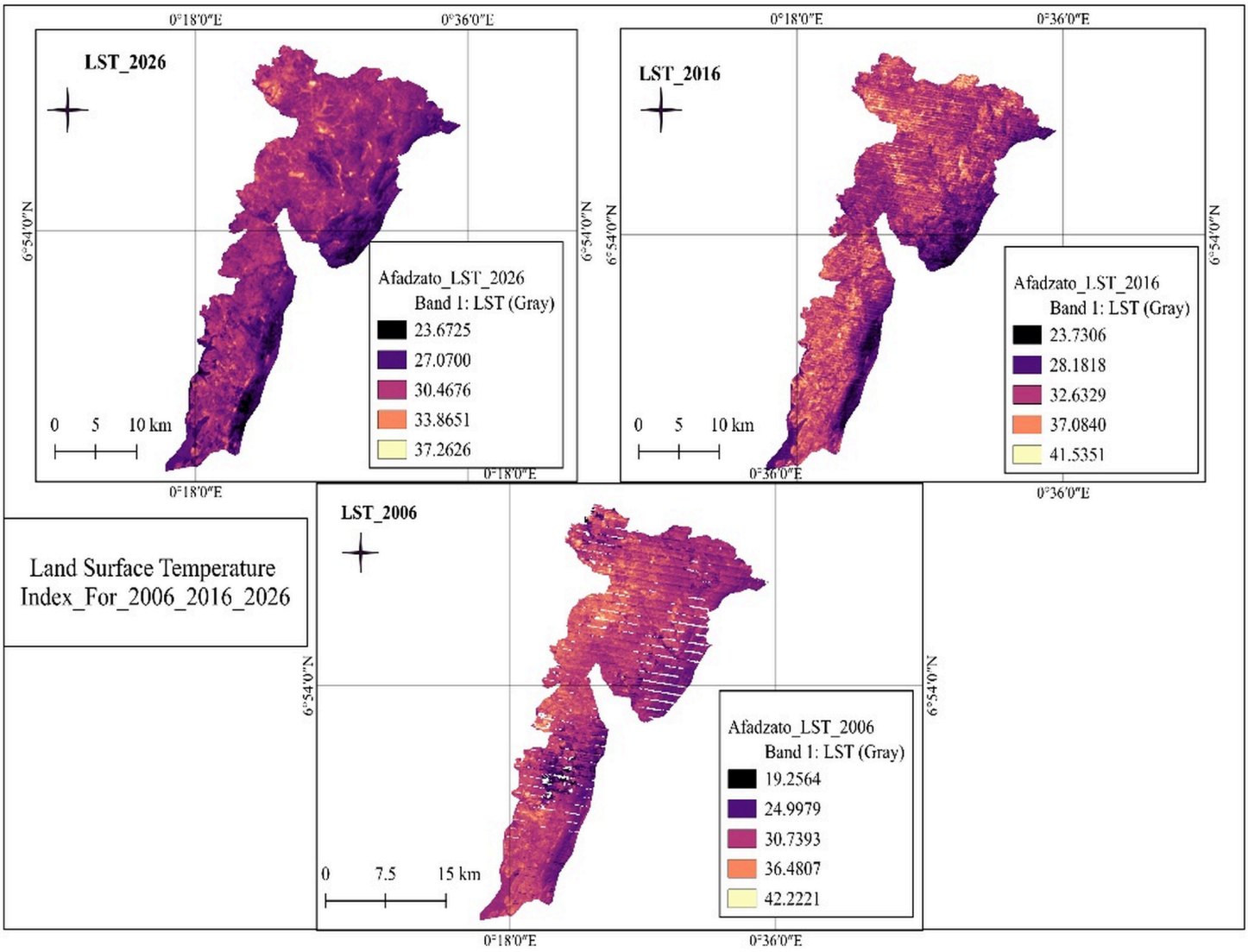


Figure 4

Dry-season land surface temperature (°C) for 2006, 2016 and 2026.

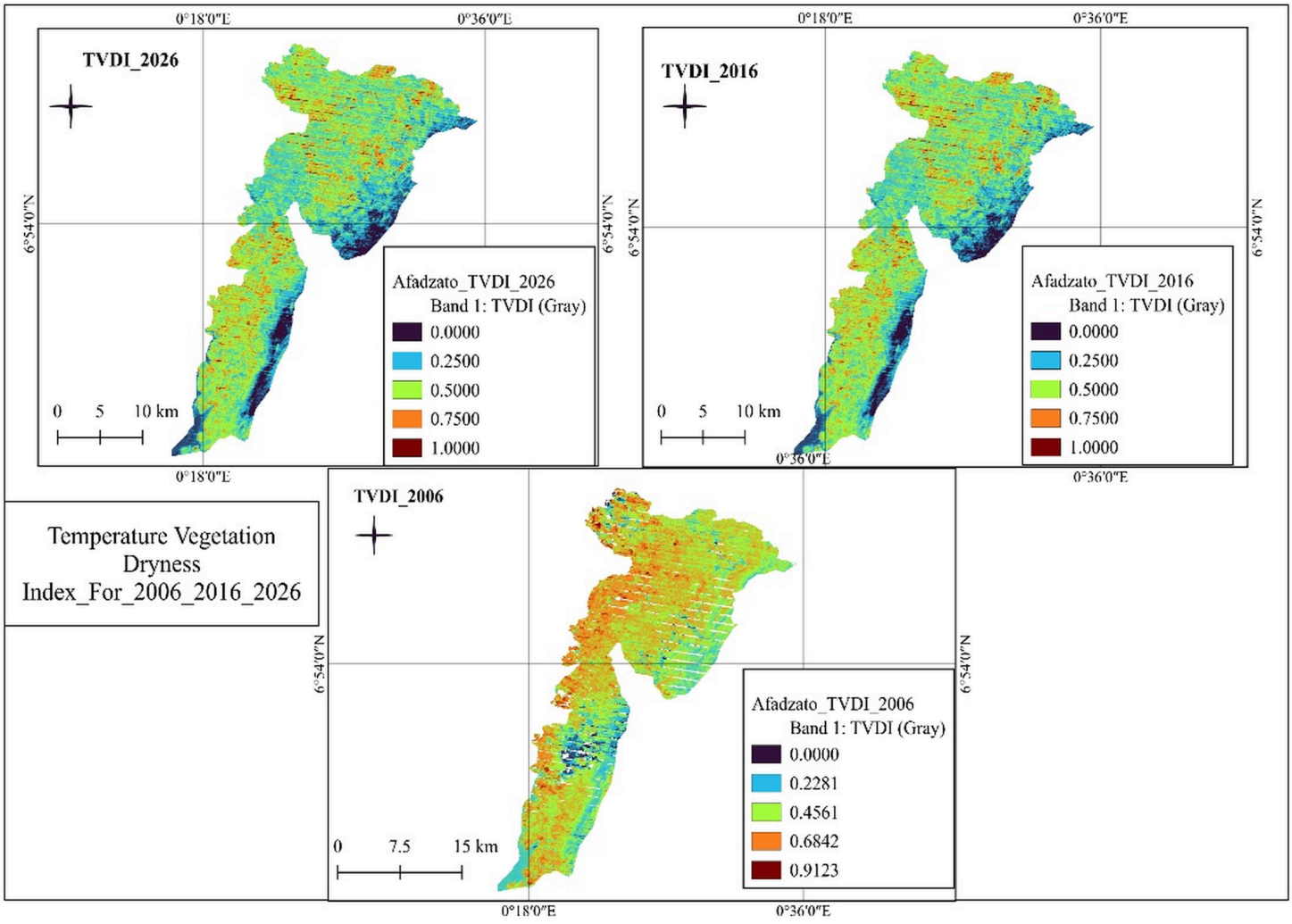


Figure 5

Dry-season TVDI for 2006, 2016 and 2026. Green–blue = wetter (low stress); orange–red = drier (high stress).

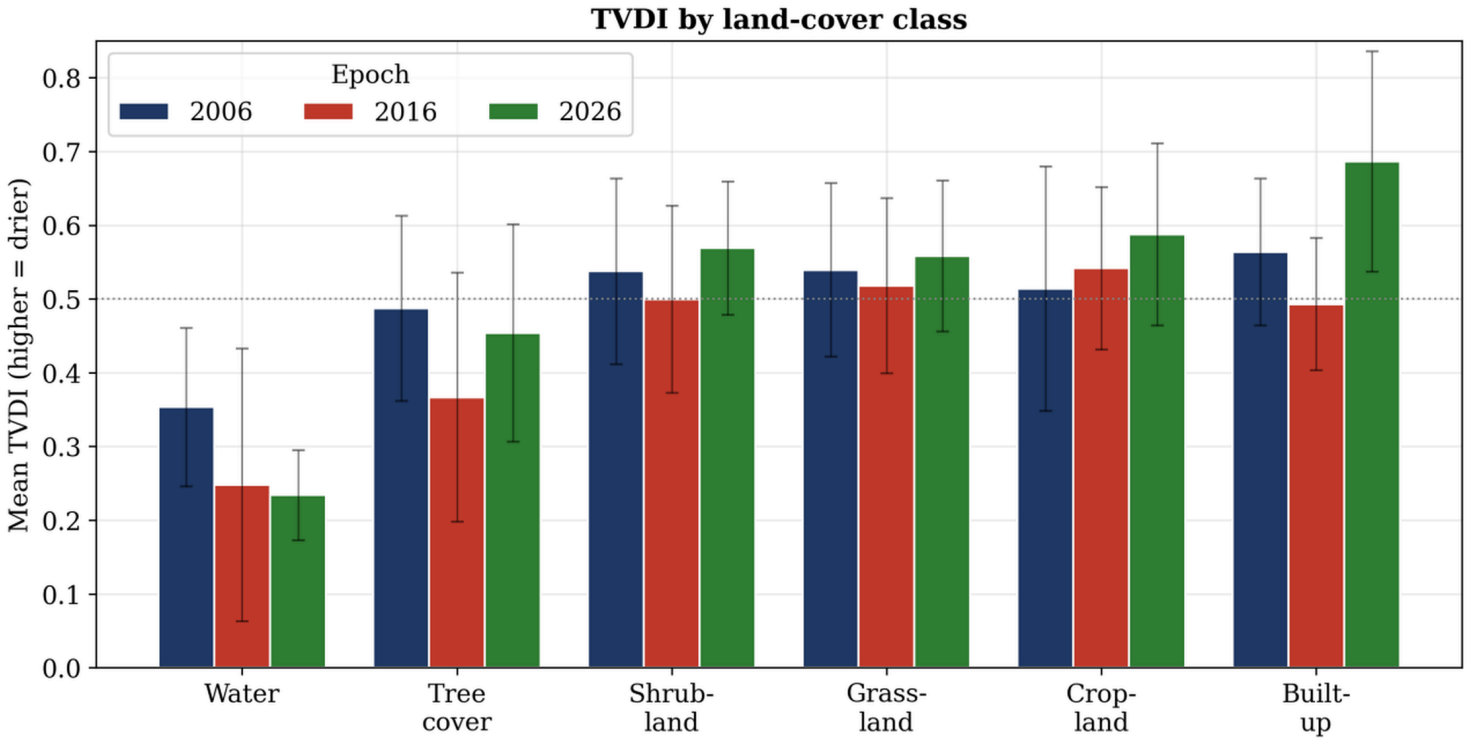


Figure 6

Mean TVDI by land-cover class for the three epochs (error bars = 1 SD; dotted line = 0.5). Water is consistently the wettest surface, built-up and cropland the driest.

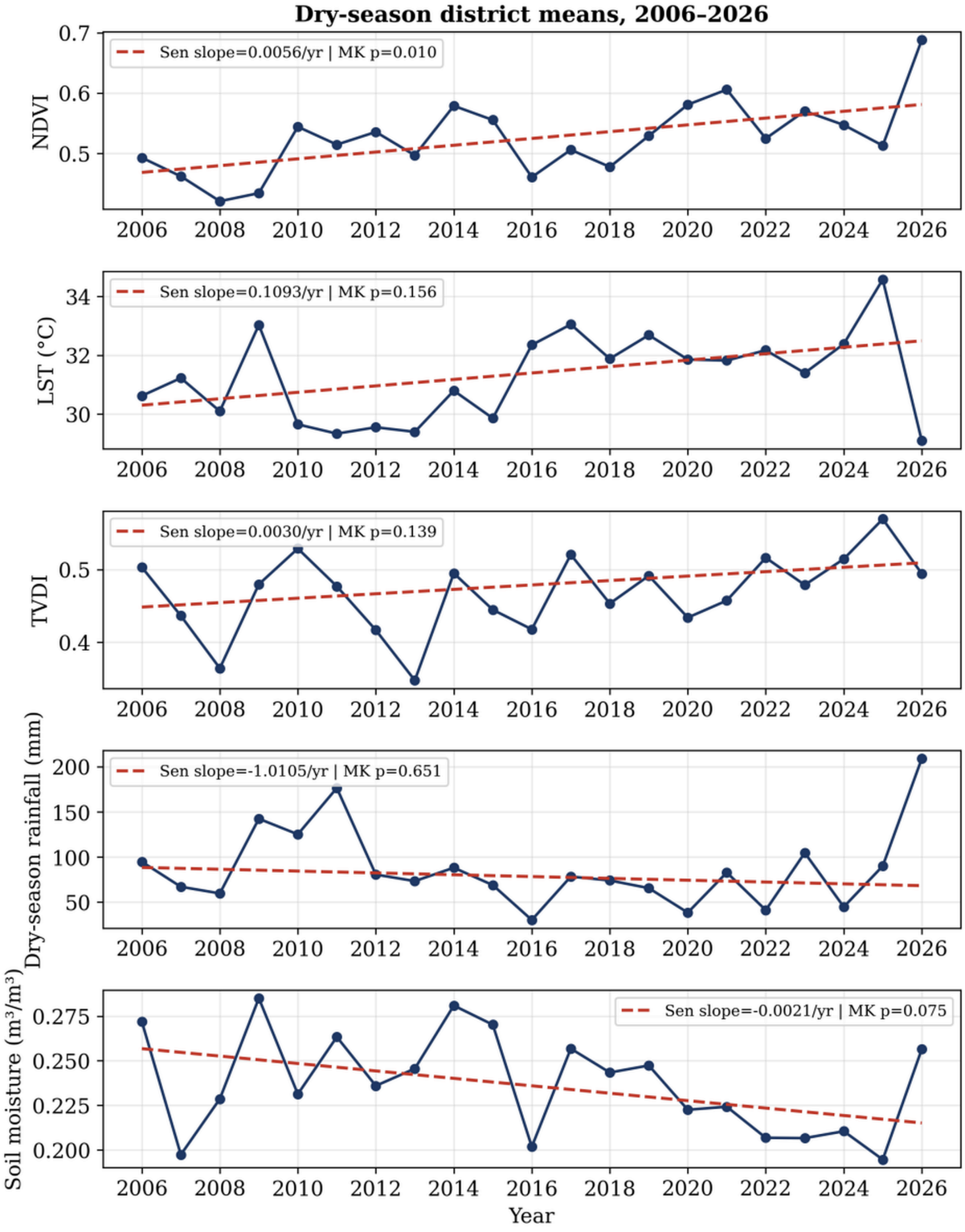


Figure 7

Dry-season district-mean time series with Sen's slope (dashed) and Mann–Kendall p-value for each variable.

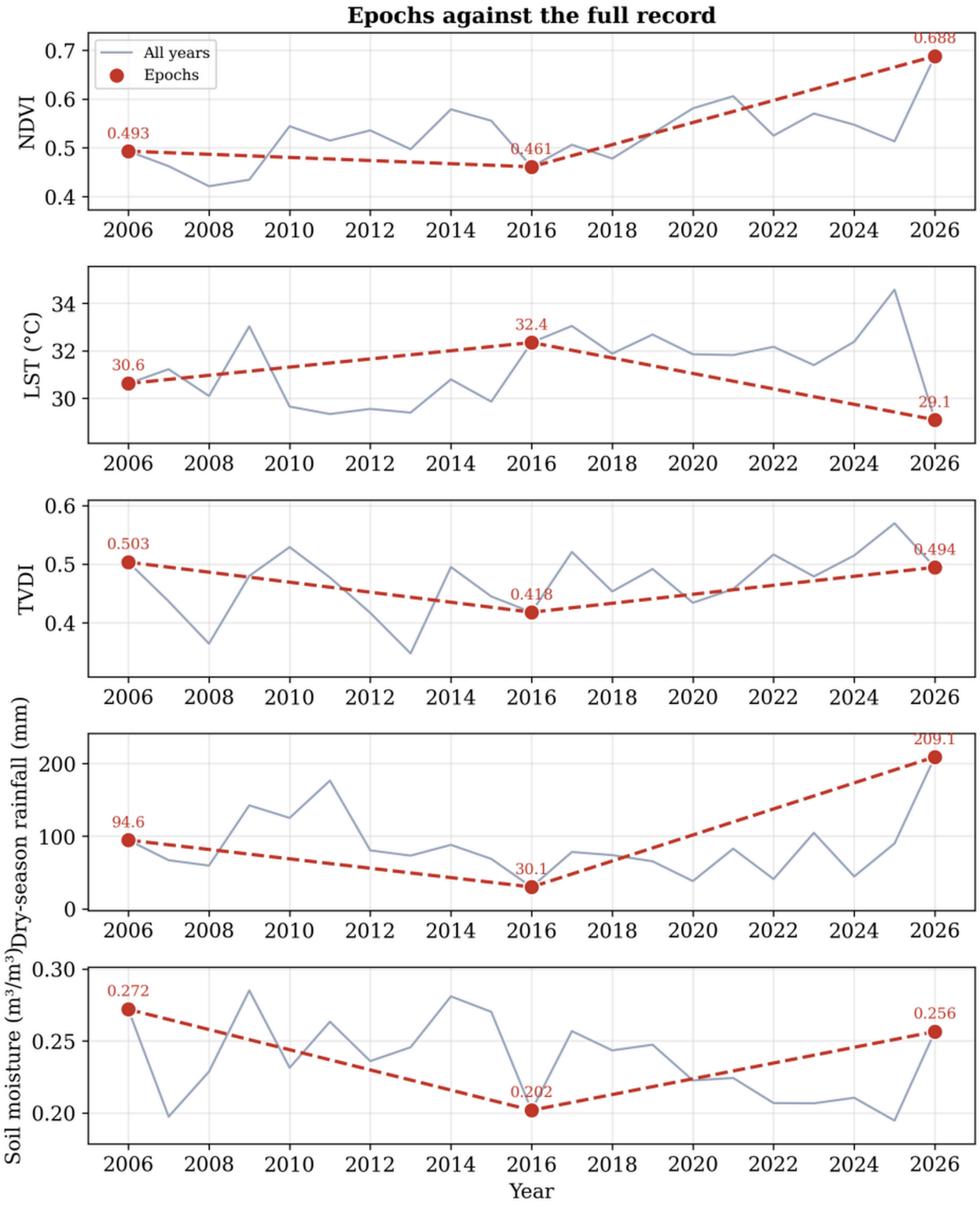


Figure 8

The three epochs (red) shown against the full 21-year record (grey); 2016 and 2026 sample the district's dry and wet extremes.

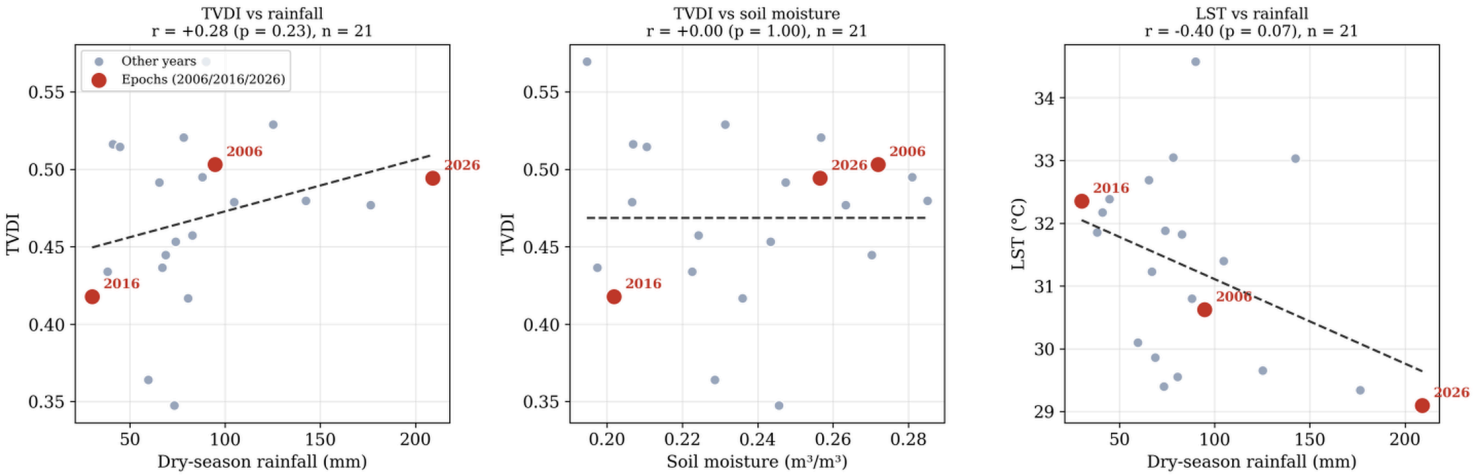


Figure 9

Validation of the indices, 2006–2026, with the three epochs highlighted. LST relates negatively to rainfall and soil moisture as expected; district-mean TVDI is a spatial rather than a temporal measure.